International Symposium
On Turbulence and Shear Flow
Phenomena (TSFP-9)
June 30 - July 3, 2015 *Melbourne, Australia*

ON THE INFLUENCE OF PRESSURE VARIATION ON IGNITION AND MIXING PROCESSES IN A REACTING SHOCK-BUBBLE INTERACTION

Felix Diegelmann
Institute for Aerodynamics and Fluid Mechanics
Technische Universität München
Boltzmannstr. 15, 85748 Garching bei München, Germany
felix.diegelmann@aer.mw.tum.de

Jan Matheis[1], Volker Tritschler[2], Stefan Hickel[3] and Nikolaus Adams[4]
Institute for Aerodynamics and Fluid Mechanics
Technische Universität München
Boltzmannstr. 15, 85748 Garching bei München, Germany

Stefan Hickel[5]
Chair of Computational Aerodynamics
Faculty of Aerospace Engineering, TU Delft
Kluyverweg 1, 2629 HS Delft, Netherlands

ABSTRACT

We present numerical simulations of a reacting shock-bubble interaction with detailed chemistry. The interaction of the Richtmyer-Meshkov instability (RMI) and shock-induced ignition of a stoichiometric H_2-O_2 gas mixture are investigated. Different initial pressures in the range of $p_0 = 0.25 - 0.75$ atm at a constant shock wave Mach number of Ma = 2.30 trigger different reaction wave types (deflagration and detonation). Low pressure reactions are dominated by H, O, OH production and high pressure chemistry is driven by HO_2 and H_2O_2. The reaction wave type is crucial for the spatial and temporal evolution of the bubble. The RMI and subsequent Kelvin Helmholtz instabilities show a high reaction sensitivity. Mixing is significantly reduced by both types of reaction waves, with detonation waves showing the strongest effect.

THEORY

In reactive flows, like in supersonic combustion, the rapid and efficient mixing of fuel and oxidizer is of crucial importance as the detention time of the fuel-oxidizer mixture in the combustion chamber is only a few milliseconds (Yang *et al.*, 1993). The Richtmyer-Meshkov instability (RMI) promotes mixing and thus has the potential to increase the burning efficiency of supersonic combustion engines (Marble *et al.*, 1990). However, the discontinuity in the thermodynamic properties can induce a reaction wave, which interacts with RMI and secondary instabilities.

RMI is a shock-induced hydrodynamic instability occurring at the separating interface of two fluids of different densities. In RMI, baroclinic vorticity production at the interface is caused by the misalignment of the pressure gradient, ∇p, associated with a shock wave, and the density gradient, $\nabla \rho$, of the material interface. For a comprehensive review the reader is referred to Brouillette (2002). The instability occurs on a wide range of scales ranging from the largest in astrophysics (Arnett, 2000), to intermediate scales in combustion (Yang *et al.*, 1993) and down to very small scales in inertial confinement fusion (Lindl *et al.*, 1992).

The shock-induced change in the thermodynamic properties can cause ignition followed by a reaction wave, where two types are differentiated: Deflagration and detonation. Deflagration is a subsonic reaction wave that propagates through the gas mixture due to a direct transfer of chemical energy from the burning to the unburned gas by diffusion (Liberman, 2008). In contrast, a detonation is driven by a faster chemical reaction and the associated large heat release within the reaction wave. A shock wave propagates directly in front of the reaction wave and preheats the gas mixture by compression (Liberman, 2008). The detonation wave propagates up to 10^8 times faster than the deflagration wave (Fickett & Davis, 2010). Due to the large difference in the characteristic reaction time scale, the reaction wave type has a crucial influence on the flow field.

RMI in combination with chemical reactions can be found in the reacting shock-bubble interactions (RSBI), an extension of the classical inert shock-bubble interaction (SBI). In this setup a planar shock wave propagates through a gas bubble, filled with a reactive gas mixture. The baro-

[1]jan.matheis@tum.de
[2]volker.tritschler@aer.mw.tum.de
[3]sh@tum.de
[4]nikolaus.adams@tum.de
[5]s.hickel@tudelft.nl

clinic vorticity generated at the interface causes the bubble to evolve into a vortex ring. Upon contact, the incident shock wave is partially reflected and partially transmitted. In case of a convergent geometry (Atwood number $A < 1$: A heavy gas bubble surrounded by light ambient gas) the transmitted shock wave travels at a slower speed than the incident shock wave. Hence, the transmitted shock wave is deformed such that it is focused at the downstream pole of the bubble. Pressure and temperature increase as the shock wave collapses in the shock focusing point, which is known as the shock-focusing phenomenon (SFP). Furthermore the vorticity deposition leads to a growth of the initial interface perturbation and, if the initial energy input is sufficiently large the flow evolves into a turbulent mixing zone through non-linear interactions of the material interface perturbations (Brouillette, 2002). Inert SBI have been rigorously studied over the last decades, see the comprehensive review of Ranjan *et al.* (2011).

First experimental investigations of a RSBI were performed by Haehn *et al.* (2012), who replaced the inert gas within the bubble by a reactive gas mixture. As the shock wave propagates through the bubble the temperature and pressure increase. This results in a raise of chemical reaction rates up to ignition of the gas mixture. In their experiment a stoichiometric gas mixture of H_2 and O_2, diluted by Xe is compressed by a shock wave with Mach numbers between $Ma = 1.34$ and $Ma = 2.83$. Depending on the shock wave strength three different conditions are achieved: No ignition within the experimental timeframe, deflagration or detonation. The reaction wave type shows a significant influence on the bubble dynamics. Haehn *et al.* (2012) provide several chemiluminescence exposures to depict the qualitative evolution of the bubble and reaction processes. Beside these exposures, they present quantitative data of the temporal evolution of the spanwise diameter of the bubble as well as the vortex ring diameter. However the complex experimental setup of Haehn *et al.* (2012) imposes significant uncertainties, underlining the necessity for a detailed numerical study of RSBI.

NUMERICAL MODEL

We solve the full set of compressible reacting multi-component Navier-Stokes equations

$$\frac{\partial \mathbf{U}}{\partial t} + \nabla \cdot \mathbf{F}(\mathbf{U}) = \nabla \cdot \mathbf{F}_v(\mathbf{U}) + \mathbf{S} \quad , \tag{1}$$

with

$$\mathbf{U} = \begin{pmatrix} \rho \\ \rho \mathbf{u} \\ E \\ \rho Y_i \end{pmatrix} \quad , \mathbf{F}(\mathbf{U}) = \begin{pmatrix} \rho \mathbf{u} \\ \rho \mathbf{u}\,\mathbf{u} + p\delta \\ (E+p)\mathbf{u} \\ \rho \mathbf{u} Y_i \end{pmatrix} \quad ,$$
$$\mathbf{F}_v(\mathbf{U}) = \begin{pmatrix} 0 \\ \tau \\ \tau \cdot \mathbf{u} - \mathbf{q}_c - \mathbf{q}_d \\ \mathbf{J}_i \end{pmatrix} \quad \text{and} \quad \mathbf{S} = \begin{pmatrix} 0 \\ \mathbf{0} \\ \dot{\omega}_T \\ \dot{\omega}_i \end{pmatrix} \tag{2}$$

with ρ representing the mixture density, $\mathbf{u}$ the velocity vector, E the total energy, p the pressure, and Y_i the mass fraction of species $i = 1,2,...N$, with N as the total number of species. τ defines the viscous stress tensor, $\mathbf{q}_c$ the heat conduction, $\mathbf{q}_d$ the interspecies diffusional heat flux, $\mathbf{J}_i$ the species diffusion and δ the identity matrix. The source term $\mathbf{S}$ in Eq. (2) represents the heat release

$$\dot{\omega}_T = -\sum_{i=1}^{N} \Delta h^0_{f,i} \dot{\omega}_i \tag{3}$$

with $h^0_{f,i}$ as the heat of formation of each species i and the species formation and destruction in terms of individual mass rates

$$\dot{\omega}_i = W_i \sum_{r=1}^{N_R} \nu_{ir} \Gamma_r \left(k_{fr} \prod_{i=1}^{N} [X_i]^{\nu'_{ir}} - k_{br} \prod_{i=1}^{N} [X_i]^{\nu''_{ir}} \right), \tag{4}$$

where N_R is the number of reactions, W_i is the molecular weight, Γ_r is the third body efficiency of reaction r, X_i the molar concentration. ν'_{ir} and ν''_{ir} are the molar stoichiometric coefficients of the reactant and the product and ν_{ir} is the net stoichiometric coefficient. The forward and backward reaction rates k_{fr} and k_{br} are calculated according to the Arrhenius law and provided by the reaction mechanism of Ó Conaire *et al.* (2004), which is validated for a wide range of pressure (0.05 to 87 atm) and temperature (298 to 2700 K). The mechanism considers $8+N$ species (two reactants: H_2, O_2; 5 chain-carrying intermediates: H, O, OH, HO_2, H_2O_2; the product: H_2O; N inert gases) and 19 intermediate reactions. High accuracy is achieved by considering pressure dependent, duplicated reactions and third body efficiencies. The mechanism has been widely used over the last years (Ferrer *et al.*, 2014). The system in (1) is solved by the 2^{nd}-order accurate Strang time splitting scheme (Strang, 1968). The Strang splitting scheme seperates the stiff source term from the Navier-Stokes equations, which results in a system of partial differential equations (PDE) and a system of stiff ordinary differential equations (ODE).

For the PDE system we use a finite-volume discretization scheme that applies a flux projection on local characteristics for the hyperbolic part. The Roe-averaged matrix required for the projection is calculated for the full multi-species system (Roe, 1981). The numerical fluxes at the cell faces are reconstructed from cell averages by the adaptive central-upwind 6^{th}-order weighted essentially non-oscillatory (WENO-CU6) scheme proposed by Hu *et al.* (2012). The fundamental idea of the WENO-CU6 scheme is to use a non-dissipative 6^{th}-order central stencil in smooth flow regions and a non-linear convex combination of 3^{rd}-order stencils in regions with steep gradients. The time integration is realized by the 3^{rd}-order total variation diminishing Runge-Kutta scheme of Gottlieb & Shu (1998). With respect to the objective in this paper the numerical model has been tested and validated for shock induced, turbulent, multi-species mixing problems at finite Reynolds numbers (Tritschler *et al.*, 2014).

The stiff ODE system is solved separately by the variable-coefficient ODE solver using 5^{th}-order backward differentiation formulas (Brown *et al.*, 1989). The present approach with Strang splitting is state-of-the-art in combustion and reactive flow simulations (Oran & Boris, 2005).

SETUP

We study RSBI on a two-dimensional rectangular domain with a symmetry plane at the center axis of the bubble,

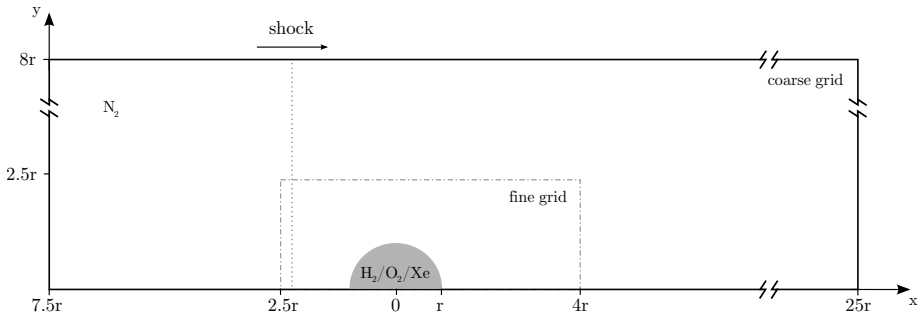

Figure 1: Schematic of the computational domain of the RSBI, r = 0.02 m.

see Fig. 1. Inflow boundary conditions are imposed on the left boundary of the domain, and outflow boundary conditions on the right and upper side. The initial bubble radius is denoted by r, and the domain size [32.5 r × 8 r] is chosen sufficiently large to avoid any effect of artificial shock reflections on the bubble evolution. Computational costs are reduced by using a fine Cartesian grid in the proximity of the bubble and a coarser grid far away from the interaction region. A grid resolution with cell sizes of $\Delta_{xy} = 59\ \mu m$ is applied in the high-resolution part of the domain. The total number of cells amounts to 2.4 million cells. Following the setup of Haehn *et al.* (2012) the bubble diameter is set to $D = 2\ r = 0.04$ m, leading to approximately 700 cells per bubble diameter. The bubble gas contains H_2, O_2 and Xe in a stoichiometric composition of 0.30 / 0.15 / 0.55 molar fractions. The inert gas Xe increases the density of the bubble, leading to an Atwood number of $A = 0.476$. The shock wave with a Mach number of $Ma = 2.3$ is initialized on the left side of the bubble. The pre-shock state is defined by $T_0 = 350$ K and three different initial pressures p_0 = 0.25 / 0.50 / 0.75 atm.

RESULTS AND DISCUSSION

Temporal and Spatial Evolution

The temporal and spatial evolution of the RSBI is highly affected by the initial pressure and the subsequent reaction wave type with its different propagation velocities. The pressure sensitivity of the chemical reactions leads to deflagration of the gas mixture at an initial pressure of p_{1_0} = 0.25 atm and to detonation for p_{2_0} = 0.50 atm and p_{3_0} = 0.75 atm. Figure 2 shows a visualization of the temporal evolution of the SBI for all cases. Three different initial pressures are compared to the baseline inert SBI at $p_{2_0} = 0.50$ atm. The contour plots show the mass fraction of Xe and H_2O in the upper half of the bubble, and the pressure in the lower half.

The characteristic stages of the inert bubble evolution are visualized in the top row of Fig. 2. At $t = 58\ \mu s$ and $t = 86\ \mu s$, the shock wave propagates through the bubble and compresses the gas mixture. At $t = 200\ \mu s$, the shock wave has passed the bubble and the primary vortex centers form, while secondary instabilities begin to evolve due to the velocity shear at the material interface. As more secondary instabilities develop and the primary vortex centers are advected downstream the mixing increases. The contour plots reveal a high degree of mixing of the bubble gas mixture with the surrounding N_2.

The three lower rows in Fig. 2 show the reacting SBI for the different initial pressures. The chemical reaction kinetics are very pressure sensitive. Hence the initial pressure variations affect distinctly the ignition delay time and the following reaction process. At the lowest pressure of $p_{1_0} = 0.25$ atm the shock wave ignites the gas mixture at $t \approx 92\ \mu s$ in the shock focusing point, which is near the downstream pole of the bubble. Here, temperature and pressure reach a maximum and a deflagration reaction wave propagates upstream through the bubble at subsonic speed. The low propagation velocity of the reaction wave causes the deflagration wave to reach the upstream pole of the bubble only at the long-term evolution at $t = 500\mu s$. The heat release associated with the chemical reaction leads to an expansion of the bubble gas. However, the influence of the subsonic deflagration wave on the bubble dynamics is limited, which can be referred from a comparison with the inert baseline case.

An increase of the initial pressure to $p_{2_0} = 0.50$ atm ignites the gas mixture slightly earlier ($t = 86\ \mu s$). The reaction wave type changes from a deflagration to a detonation wave, which propagates through the unburned bubble gas in $t \approx 14\ \mu s$ at supersonic speed. The detonation reaction wave drives a shock wave in front of it, which results in a significant increase in pressure. The strong heat release and the pressure raise result in a rapid bubble expansion. When the detonation wave reaches the material interface of the bubble, baroclinic vorticity with opposite sign is generated. This leads to a suppression of secondary instabilities, which develop as a consequence of the velocity shear across the material interface, as can be seen in Fig. 2 at $t = 200\ \mu s$ and $t = 400\ \mu s$. The detonation wave amplifies the N_2-jet that forms at the symmetry plane at the downstream pole of the bubble at $t = 200\ \mu s$. The amplified jet breaks through the bridge at the upstream pole of the bubble that connects the two primary vortices.

The further increase of the initial pressure to $p_{3_0} = 0.75$ atm has no significant effect on the spatial and temporal evolution of the bubble at early times. The gas mixture ignites 2 μs earlier, compared to an initial pressure of $p_{2_0} = 0.50$ atm, and the propagation velocity of the detonation wave is similar. Hence, the long-term evolution is nearly unaffected by a further increase of pressure, once a pressure limit is exceeded and transition to detonation is achieved.

The occurrence of either a detonation or a deflagration reaction wave can be explained by the pressure sensitivity of the H_2-O_2 reaction kinetics. At identical temperatures in the shock focusing point the different initial pressure triggers different reaction waves. Deflagration is characterized by

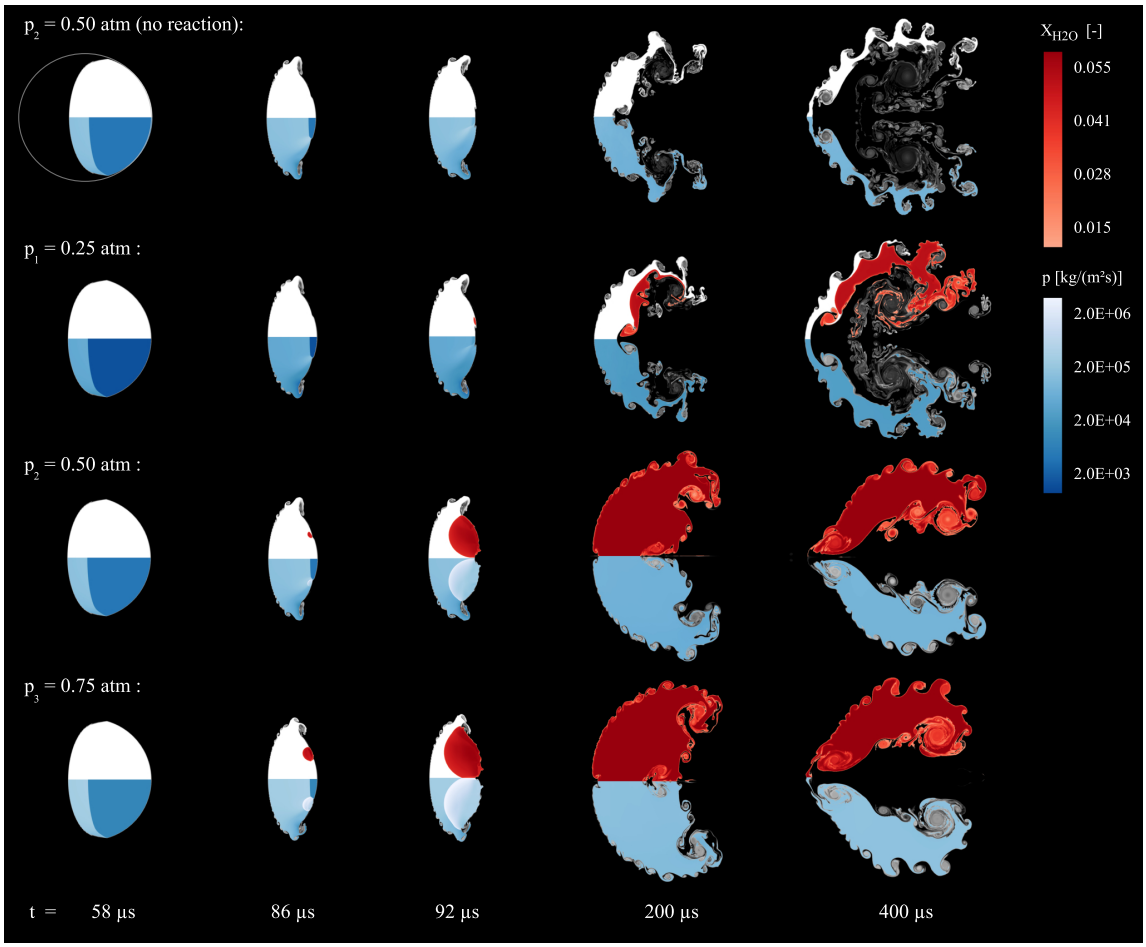

Figure 2: Chemical kinetics in RSBI: Upper part shows mass fraction of the inert gas Xe (gray scale) and the product H_2O (red color scale), illustrating the reaction wave. Lower part depicts the characteristic pressure distribution.

the dominant production of H, O and OH radicals, whereas detonation is accompanied by a higher formation of HO_2 and H_2O_2. The chain-carrying radicals get accumulated until ignition of the gas mixture.

Damköhler number

The influence of the chemical reaction on the flow field is determined by the dimensionless Damköhler number, which defines the ratio of hydrodynamic and chemical reaction time scales

$$Da = \frac{\tau_h}{\tau_r}. \tag{5}$$

Da < 1 characterizes a flow field dominated by hydrodynamic effects, Da > 1 implies a high influence of the chemical reaction. The two time scales are defined as follows:

$$\tau_h = \frac{1}{|\overline{\omega}|} \quad , \quad \tau_r = \tau_{ign} + \frac{D_0}{V_{RW}} \quad . \tag{6}$$

The characteristic hydrodynamic time scale τ_h is defined by the vorticity, averaged over the propagation time of the reaction wave inside the bubble. The chemical reaction time τ_r scale consists of two time intervals: τ_{ign} is the period from the first contact of the shock with the bubble until ignition. D_0/V_{RW} is the time the reaction wave takes to propagate through the initial bubble shape with D_0 as the initial bubble diameter. V_{RW} is the propagation velocity of the reaction wave. The Damköhler numbers for the different initial pressures of the RSBI are listed in Tab. 1.

Table 1: Damköhler numbers and characteristic time scales for different initial pressures.

p_{x_0} $[atm]$	τ_h $[s]$	τ_r $[s]$	Da $[-]$
0.25	$0.4296 \cdot 10^{-3}$	$1.4203 \cdot 10^{-3}$	0.3025
0.50	$0.1889 \cdot 10^{-3}$	$0.0679 \cdot 10^{-3}$	2.7834
0.75	$0.1864 \cdot 10^{-3}$	$0.0659 \cdot 10^{-3}$	2.8309

For the subsonic deflagration wave, induced at a low initial pressure of $p_{1_0} = 0.25$ atm, we find $Da = 0.3025$. The characteristic time scale of the chemical reaction kinetics τ_r is higher than the hydrodynamic time scale τ_h. Consequently the flow field is dominated by hydrodynamic ef-

fects. The instabilities at the interface and in the main vortex regions evolve nearly unaffected from the propagating deflagration wave, as visualized in Fig. 2.

An increase of the initial pressure changes the reaction-wave type to a supersonic detonation wave. Due to the fast propagation velocity, the chemical reaction time scale decreases distinctly and becomes smaller than the hydrodynamic time scale. Thus the chemical reaction plays a crucial role for the overall bubble dynamics. This is reflected by an increase of the Damköhler number to $Da = 2.7834$. A further increase of the initial pressure up to $p_{3_0} = 0.75$ atm reduces the induction time slightly by about 2 μs, leading to a Damköhler number of Da = 2.8309. The similarity of the Damköhler numbers for an initial pressure $p_{x_0} \geq 0.50$ atm indicates that once a critical initial pressure is exceeded the domination of the chemical reaction time scale becomes pressure independent. The following analysis of integral quantities supports this observation.

Enstrophy generation and mixing

The analysis of the enstrophy indicates the influence of the reaction wave on the vorticity production during the SBI. The baroclinic vorticity production term $(\nabla\rho \times \nabla p)/\rho^2$ produces vorticity right after the shock wave first contacts the upstream pole of the bubble. If the gas mixture detonates, the supersonic reaction wave acts as a second shock wave and induces additional vorticity. The enstrophy ε_ρ is used to determine the influence of the different reaction waves, in particular of the detonation wave, on the vorticity production

$$\varepsilon_\rho = \frac{1}{\rho_0}\,\varepsilon = \frac{1}{\rho_0}\int_S \rho\,\omega^2\,dx\,dy. \tag{7}$$

As the simulations are initiated with different initial pressures and therefore different densities, the enstrophy is normalized by the respective initial density ρ_0. Figure 3 shows the temporal evolution of the enstrophy for the simulations of RSBI and their non-reacting counterparts. Vorticity production starts with the first contact of the shock wave with the bubble at t = 30 μs and increases during the shock passage. The evolution is identical for the reacting and non-reacting simulations until ignition occurs at $t \approx 86$ μs. The detonation wave induces additional vorticity. The corresponding enstrophy peak is clearly visible in Fig. 3 and leads to elevated enstrophy levels for a time period of about 50 μs. In the long-term evolution, the non-reacting SBIs show higher enstrophy levels than the reacting simulations because of a higher density and pressure gradient in the main vortex region. The deflagration wave has only a small influence on the enstrophy. After the reaction wave has reached a significant part of the interface, however, the vorticity decays faster compared to the inert counterpart. Again the reason can be found in the decrease of the density over the reaction front.

The molecular mixing fraction (MMF), defined by Youngs (1994), is used to estimate the mixing in a complex flow field dominated by RMI and Kelvin Helmholtz instabilities (KHI)

$$\Theta(t) = \frac{\int_{-\infty}^{\infty} \langle X_{N_2} X_{Xe} \rangle\,dx}{\int_{-\infty}^{\infty} \langle X_{N_2} \rangle \langle X_{Xe} \rangle\,dx}. \tag{8}$$

The MMF quantifies the amount of mixed fluid within the

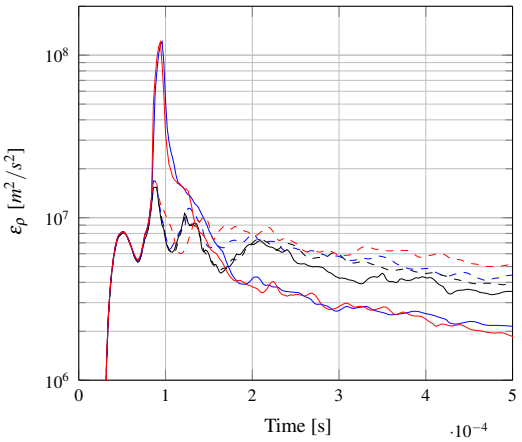

Figure 3: Enstrophy normalized by the respective initial density. Solid lines: reaction; dashed lines: no reaction; —— / - - - p_{1_0} = 0.25 atm, —— / - - - p_{2_0} = 0.50 atm, —— / - - - p_{3_0} = 0.75 atm.

mixing zone. It can be interpreted as the ratio of molecular mixing to large-scale entrainment by convective motion. Tomkins *et al.* (2008) observed three main regions of mixing: The vortex core, the outer interface including KHI, and the bridge region connecting the two main vortices. The latter contributes up to 40% to the mixing. The temporal evolution of MMF of the reacting simulations and the non-reacting counterparts are plotted in Fig. 4.

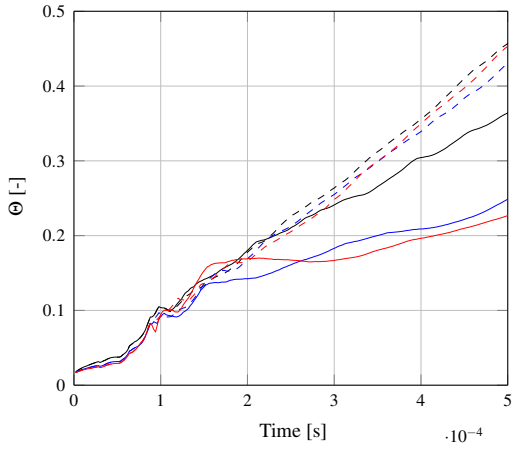

Figure 4: Molecular mixing fraction. Solid lines: reaction; dashed lines: no reaction; —— / - - - p_{1_0} = 0.25 atm, —— / - - - p_{2_0} = 0.50 atm, —— / - - - p_{3_0} = 0.75 atm.

The inert simulations show a linear growth over time, which is independent of the initial pressure. The reacting counterpart, on the other hand, shows a different behavior. The low pressure simulation diverges only slightly from the inert cases. The mixing in the vortex core region and the outer interface is gradually affected by the deflagration

wave. The stretching of the bubble gas around the vortex cores and the interfacial area is less developed, which reduces the mixing. Due to the low propagation velocity of the reaction wave the bridge region at the upstream pole of the bubble, as the main mixing region, is unaffected by the chemical reaction process. For higher initial pressures, leading to a detonation wave, we observe a stronger effect of chemical reactions on the MMF. Besides the reduction of mixing in the vortex core region and at the interface, the bridge region is also highly affected by the reaction wave. The connection of the two main vortices is disturbed. Thus, the MMF of the high pressure simulations is reduced by up to 50% within the simulations timeframe, see Fig. 4. Note that, the increase in the initial pressure is only important to obtain detonation. Once the reaction wave propagates with supersonic speed, a further pressure raise shows no significant influence on the MMF. In general, the MMF is reduced by the chemical reaction, especially the supersonic combustion decreases the mixing distinctly.

CONCLUSION

We have presented results from the first numerical simulation of a reacting shock-bubble interaction (RSBI) with detailed H_2-O_2 chemical reaction kinetics. We considered a bubble filled with a stoichiometric gas mixture of H_2, O_2 and Xe, surrounded by pure N_2. A planar shock wave propagates through the domain and interacts with the spherical density inhomogeneity, which leads to Richtmyer-Meshkov instability (RMI). Shock focusing causes ignition of the bubble gas. We were able to show that the pressure sensitivity of the H_2-O_2 reaction can be used to control the reaction wave type through variation of the initial pressure. A deflagration or a detonation wave can be triggered, which highly affects the efficiency of the mixing process in a RSBI. In a low pressure environment the production of H, O, OH radicals dominates, leading to a subsonic deflagration wave. Higher initial pressures lead to a chemical reaction driven by HO_2 and H_2O_2 resulting in a supersonic detonation wave.

The spatial and temporal evolution of the reacting shock-bubble interaction are highly affected by the reaction wave type. A subsonic deflagration wave leads to a flow field dominated by hydrodynamic effects ($Da \approx 0.3$), thus the influence of the reaction wave on the global bubble evolution is small. Secondary instabilities evolve unaffected by the reaction wave. The mixing decreases by about 20% within the timeframe of the simulation. The second reaction wave type, the detonation wave, leads to a flow field dominated by chemical reaction time scales ($Da \gtrsim 2.78$). The bubble gas expands quickly due to the supersonic propagation velocity of the reaction wave. Enstrophy production increases distinctly but decays faster. The growth of the secondary instabilities is suppressed and the mixing regions are highly affected by the chemical reaction. The molecular mixing fraction reduces by up to 50% compared to the inert case.

ACKNOWLEDGEMENT

The authors gratefully acknowledge the Gauss Centre for Supercomputing e.V. (www.gauss-centre.eu) for providing computing time on the GCS Supercomputer SuperMUC at Leibniz Supercomputing Centre (LRZ, www.lrz.de).

REFERENCES

Arnett, W. D. 2000 The Role of Mixing in Astrophysics. *The Astrophysical Journal Supplement Series* **127**, 213–217.

Brouillette, M. 2002 The Richtmyer-Meshkov Instabilty. *Annual Review of Fluid Mechanics* **34**, 445–468.

Brown, P. N., Byrne, G. D. & Hindmarsh, A. C. 1989 Vode: A variable-coefficient ode solver. *SIAM Journal on Scientific and Statistical Computing* **10** (5), 1038–1051.

Ferrer, P. J. M., Buttay, R., Lehnasch, G. & Mura, A. 2014 A detailed verification procedure for compressible reactive multicomponent Navier-Stokes solvers. *Computers & Fluids* **89**, 88–110.

Fickett, W. & Davis, W. C. 2010 *Detonation: Theory and Experiment*. Dover Publications.

Gottlieb, S. & Shu, C.-W. 1998 Total variation diminishing Runge-Kutta schemes. *Mathematics of Computation* **67**, 73–85.

Haehn, N., Ranjan, D., Weber, C., Oakley, J., Rothamer, D. & Oakley, R. 2012 Reacting shock bubble interaction. *Combustion and Flame* **159** (3), 1339–1350.

Hu, X. Y., Tritschler, V. K., Pirozzoli, S. & Adams, N. A. 2012 Dispersion-dissipation condition for finite difference schemes. *ArXiv e-prints* .

Liberman, M. 2008 *Introduction to Physics and Chemistry of Combustion: Explosion, Flame, Detonation*. Springer.

Lindl, J. D., McCrory, R. L. & Campbell, E. M. 1992 Progress toward Ignition and Burn Propagation in Inertial Confinement Fusion. *Physics Today* **45** (9), 32–40.

Marble, F., Zukoski, E., Jacobs, J., Hendricks, G. & Waitz, I. 1990 Shock Enhancement and Control of Hypersonic Mixing and Combustion. In *AIAA 26th Joint Propulsion Conference, Orlando*.

Ó Conaire, M., Curran, H. J., Simmie, J. M., Pitz, W. J. & Westbrook, C. K. 2004 A comprehensive modeling study of Hydrogen oxidation. *International Journal of Chemical Kinetics* **36**, 603–622.

Oran, E. & Boris, J. 2005 *Numerical Simulation of Reactive Flow*. Cambridge University Press.

Ranjan, D., Oakley, J. & Bonazza, R. 2011 Shock-Bubble Interactions. *Annual Review of Fluid Mechanics* **43** (1), 117–140.

Roe, P. L. 1981 Approximate Riemann solvers, parameter vectors, and difference schemes. *Journal of Computational Physics* **43**, 357–372.

Strang, G. 1968 On the Construction and Comparison of Difference Schemes. *SIAM Journal on Numerical Analysis* **5** (3), 506–517.

Tomkins, C., Kumar, S., Orlicz, G. & Prestridge, K. 2008 An experimental investigation of mixing mechanisms in shock-accelerated flow. *Journal of Fluid Mechanics* **611**, 131–150.

Tritschler, V. K., Olson, B. J., Lele, S. K., Hickel, S., Hu, X. Y. & Adams, N. A. 2014 On the RichtmyerMeshkov instability evolving from a deterministic multimode planar interface. *Journal of Fluid Mechanics* **755**, 429–462.

Yang, J., Kubota, T. & Zukoski, E. 1993 Applications of shock-induced mixing to supersonic combustion. *AIAA Journal* **31**, 854–862.

Youngs, D.L. 1994 Numerical simulation of mixing by Rayleigh-Taylor and Richtmyer-Meshkov instabilities. *Laser and Particle Beams* **12**, 725–750.